Multistatic Sensing for Target Localization in ISAC Systems with Dynamic and Unknown-Location Transmitters

Shun Zhuge, *Student Member*, *IEEE*, Yugang Ma, *Senior Member*, *IEEE*, Zhiping Lin, *Life Senior Member*, *IEEE*, and Yonghong Zeng, *Fellow*, *IEEE*

***Abstract*—Current research on integrated sensing and communication (ISAC) primarily examines the use of communication waveforms to derive radar parameters, but there is a significant gap in methods for accurately locating targets using these parameters. Therefore, this paper explores target localization solutions within an ISAC system under two scenarios. First, we investigate tracking a moving target using multistatic sensing with dynamic transmitters (TXs). Unlike existing two-step weighted least square (2SWLS) methods, which rely on the bistatic range (BR) and bistatic range rate (BRR) measurements, our method incorporates an additional direction of arrival (DOA) measurement. This innovation reduces the minimum number of required transmitter-receiver (TX-RX) pairs, needing only one TX-RX pair for position estimation and two TX-RX pairs for velocity estimation, thereby improving system efficiency and accuracy. In the second scenario, we address the challenge of unknown-location TXs. We pioneer a novel method that simultaneously tracks the moving target and determines the locations of these unknown-location TXs. This approach operates effectively with only three TX-RX pairs, overcoming the significant obstacle of operating without prior knowledge of TX positions. Simulations validate the effectiveness of our proposed methods. For the first scenario, our method demonstrates superior performance compared to existing 2SWLS methods. For the second scenario, our method successfully navigates the complexity of unknown-location TXs, achieving reliable target tracking and TX localization. As a result, this paper fills the gap in current ISAC studies by providing detailed methods for accurately locating a target using radar parameters obtained from an ISAC receiver.**

***Index Terms*—Integrated sensing and communication (ISAC), multistatic sensing, localization, range rate estimation**

I. Introduction

INTEGRATED sensing and communication (ISAC) is is emerging as a crucial enabling technology for future wireless communication networks, including beyond 5G (B5G) and 6G [1]–[12]. Various terminologies like dual functional of radar and communication (DFRC), joint radar and communication (JRC), and joint communication and sensing (JCAS) are sometimes used interchangeably with ISAC. The defining feature of ISAC lies in its ability to employ a single ISAC waveform for both communicating with user equipment (UE) and simultaneously sensing the target [5].

Traditionally, conventional communication signals were inadequate for radar applications due to their limited signal bandwidth and data carrier waveform [5], [6]. However, recent advancements in communication and sensing technologies [6]–[10], particularly in 5G and ISAC [13]–[15], have ushered in the use of broader signal bandwidths, massive multiple-input and multiple-output (mMIMO), and reconfigurable intelligent surfaces (RIS) techniques, enabling range resolution of less than 1 m, velocity resolution of 0.1 m/s, and angular resolution of 1° [6]–[8]. These accurate estimations of range, speed, and angle have achieved comparable performances to dedicated radar [7]–[10]. Thus, using the same communication waveform for achieving both communication and sensing functions is viable [8], [12]–[14]. To address the objective of achieving high location accuracy within the ISAC framework, this paper delves into the challenge of target localization in an ISAC system under multistatic sensing conditions.

A. Multistatic ISAC

Performing sensing in an ISAC system using a traditional monostatic radar approach presents a significant drawback [16]. In monostatic ISAC systems, where transmission and receiving antennas are co-located, strong self-interference from the transmitter (TX) to the radar receiver (RX) is inevitable [8], [17], [18]. This interference can substantially degrade radar sensing performance, resulting in reduced accuracy. Bistatic sensing offers a more advantageous alternative within the ISAC framework. In bistatic ISAC systems, sensing signals are transmitted and received by antennas located at different positions [19]–[23], effectively minimizing mutual interference and enhancing the accuracy of parameter estimation. Moreover, by employing multiple distributed TXs and RXs, a bistatic ISAC system can evolve into a multistatic ISAC system [21]–[23].

B. Overview of Related Works

Multistatic sensing offers several advantages beyond eliminating self-interference, including reduced probability of being detected, cost-effectiveness, and access to diverse transmitters TXs [22]–[24], making it a highly researched area. Over recent decades, numerous localization algorithms based on multistatic sensing scenarios have been proposed [20], [24]–[39]. Common target localization methods in multistatic sensing take two steps. First, the system extracts intermediate

This research is supported by the National Research Foundation, Singapore and Infocomm Media Development Authority under its Future Communications Research Development Programme (Grant award number: FCP-ASTAR-TG-2022-003). (Corresponding author: Yugang Ma.)

Shun Zhuge and Zhiping Lin are with the School of Electrical and Electronic Engineering, Nanyang Technological University, 639798, Singapore (e-mail: szhuge002@e.ntu.edu.sg; ezplin@ntu.edu.sg).

Yugang Ma and Yonghong Zeng are with the Institute for Infocomm Research, Connexis 138632, Singapore (e-mail: mayg@a-star.edu.sg; yhzeng@ieee.org).

Shun Zhuge is now with the Faculty of Electrical Engineering, Mathematics and Computer Science, Delft University of Technology, Delft 2628 CD, The Netherlands.

measurements, including received signal strength (RSS) [31], [33], time of arrival (TOA) [33], [35], time difference of arrival (TDOA) [27], [29], [30], [34], frequency difference of arrival (FDOA) [31], and direction of arrival (DOA) [27], [31], from received signals. Then, the localization problem is transformed into solving a nonlinear and nonconvex optimization problem related to these intermediate measurements [25].

Many existing methods are inspired by the well-known two-step weighted least square method (2SWLS) in [34] and use bistatic range (BR) and bistatic range rate (BRR) measurements, which are derived from TDOA and FDOA measurements. Reference [25] proposed a 2SWLS-based closed-form solution that achieves the Cramér-Rao lower bound (CRLB) accuracy in locating the target position with BR measurements. Reference [35] introduced a 2SWLS method in which an auxiliary variable is introduced to retain numerical stability regarding the relative geometry of the TXs, RXs, and targets. In [24], an improved 2SWLS closed-from method is proposed that outperforms methods in [25], [35]. References [36] and [38] extend the research method in [24] by investigating a moving target in the presence of position uncertainties in TXs. The study in [38] is further extended in [39] to equip the localization method with a new ability to estimate the acceleration of a uniformly accelerated moving object by using an additional bistatic acceleration (BA) measurement. However, all those methods have some limitations. First, 2SWLS methods require a minimum of three transmitter-receiver (TX-RX) pairs for operation which may affect their practicality when available pairs are limited in practice. Second, most methods consider multiple RXs to enhance estimation accuracy without considering the drawbacks of distributed RXs such as communication among RXs, computational capability of RXs, clock synchronization [37], etc. Third, most existing methods assume that the status of TXs, such as location and velocity, are perfectly known in the receiver, which limits their practical applicability. While [36] and [38] consider the position uncertainties in TXs, they still utilize the inaccurate TX positions for initial estimation, rather than treating the transmitter positions as unknown information. Additionally, there is a lack of clarity regarding the methods used to obtain these inaccurate TX positions. Finally, in consideration of the evolution of communication technologies, the ISAC receiver may be capable of detecting a greater number of radar parameters simultaneously, including not only BR and BRR but also additional parameters. Reference [39] introduces the BA to enhance the functionality of the RX, yet there is no discernible improvement in localization performance when compared to methods that solely utilize BR and BRR measurements. It is possible that the localization performance could be enhanced by employing a greater number of parameters for estimation, rather than solely relying on BR and BRR measurements.

C. Our Contributions

Motivated by the aforementioned limitations and gaps, we aim to propose a novel target localization solution in an ISAC system through multistatic sensing with advanced performance and functionality. As previously outlined in [20], our earlier research introduced a multistatic ISAC system built upon the standardized 5G new radio (NR) waveform. The transmitted signal contains modulated data, which allows the communication RX to receive useful communication data while performing the sensing function simultaneously. In this proposed decision feedback bistatic architecture, the RX first estimates the channel based on pilots/preambles, then demodulates and decodes the signal for communication purposes, and finally uses the recovered signal samples for radar sensing. The range and speed parameters are estimated based on the range-Doppler map (RDM) constructed by the decision feedback. Furthermore, a novel DOA estimation algorithm is proposed, based on the RDM and fast Fourier transform (FFT). Consequently, the system proposed in [40], [41] is capable of simultaneously detecting the BR, BRR, and DOA of the target, thereby functioning as a radar while performing the communication function. Nevertheless, our previous work in [20] solely addressed the estimation of radar parameters (range, speed, and angle), with the localization algorithm remaining unaddressed. Consequently, our previous work in [40] proposed the multistatic sensing algorithm for the purpose of locating a moving target within the ISAC system, utilizing the aforementioned radar parameters obtained from [20]. In [40], we propose a novel representation of the geometric relationships among TXs, the target, and the RX and a new multistatic sensing algorithm that requires only one TX-RX pair to estimate the target position and only two TX-RX pairs to estimate the target velocity. Although our proposed method in [40] overcomes some limitations in existing 2SWLS methods, such as the minimum number of required TX-RX pairs and the consideration of multiple RXs, it still relies on some constrained assumptions. In [40], the ISAC system assumes that the TXs are static, and the positions of the TXs are perfectly known to the RX. However, in practice, the TXs can also be mobile, and the RX may not know the exact positions of the TXs.

To address above issues, this paper focuses on target localization in a multistatic ISAC system with dynamic and unknown-location TXs, where the dynamic TX is defined as a TX whose location is time varying. This work focuses on the geometric estimation stage, which operates after the BR, BRR, and DOA measurements have been obtained at the RX side. The objective is to analyze how these measurements—regardless of the specific sensing front-end, waveform, or DOA estimation method used to generate them—can be jointly exploited to recover the desired target states under representative multistatic ISAC scenarios. Accordingly, this paper does not propose new signal-processing or DOA estimation techniques, nor does it model the sensing hardware; instead, it concentrates on the downstream geometric inference problem built upon these measurements. The major contributions of this paper are outlined below:

- A novel multistatic sensing algorithm for an ISAC system with dynamic TXs. This algorithm requires only one TX-RX pair to estimate the target position and three TX-RX pairs to estimate the target velocity. In contrast, the existing 2SWLS methods must use at least three TX-RX pairs to locate a target.

- To the best of our knowledge, the proposed method is the first multistatic sensing algorithm for an ISAC system with unknown-location TXs. This algorithm overcomes the limitation of the required position information for TXs. By using a minimum of four TX-RX pairs, the proposed algorithm can estimate the target position, target velocity, and TX positions at the same time.

Compared with the existing localization method in [24] under the same number of TX-RX pairs, our proposed method for an ISAC system with dynamic TXs can achieve lower root-mean-square error (RMSE) in both position and velocity estimation at a moderate estimation error of DOA.

The remainder of this paper is organized as follows. In Section II, we formulate the multistatic sensing problem of a moving target in ISAC systems with consideration of dynamic TXs and unknown-location TXs separately. The proposed algorithms are presented in Section III. Section IV gives the simulation results and discussions. Finally, some conclusions are drawn in Section V.

II. System Model

This section introduces the three-dimensional (3D) measurement model for the ISAC system illustrated in Fig. 1. In this setup, the communication TXs emit 5G NR–compliant modulated signals, which propagate simultaneously toward the ISAC RX via the direct path and toward the unknown moving targets, where they are reflected back to the RX. To avoid complications related to inter-receiver communication, time synchronization, and distributed calibration, we consider a single ISAC RX in this system. Moreover, our approach does not require strict synchronization among the transmitters; it only assumes that the target location remains approximately unchanged during the reception of signals from different TXs. The RX, equipped with an antenna array, receives both the direct and reflected paths, enabling it to function as a radar sensor capable of extracting BR, BRR, and DOA associated with the targets [20]. In addition, no specific target type is assumed, as the sensing front-end and target scattering mechanisms are not modeled; instead, the formulation focuses solely on the geometric relationships among the TXs, the RX, and the targets. As an additional DOA measurement is incorporated, the model is formulated in spherical coordinates. Based on the geometric relationships among the TXs, RX, and targets, expressions for both the range and range rate are derived. For clarity and consistency in vector operations—such as dot products and projections—certain intermediate steps convert spherical coordinates to Cartesian coordinates. These conversions are solely for computational convenience, and all final expressions are presented in spherical form.

Two different multistatic sensing scenarios are considered under the unified system. Section II-A discusses the case where the TXs are dynamic, i.e., moving with certain velocities, while Section II.B addresses the case where the TXs are static, but their positions are unknown to the RX. Measurement noise is incorporated into the model in Section II.C. Lastly, Section II.D explains how the multi-target localization problem can be decomposed into a set of independent per-target subproblems to facilitate algorithm design and analysis.

A. Model with Dynamic TXs

We first consider the multistatic sensing problem aimed at tracking multiple moving targets in an ISAC system with dynamic TXs. As illustrated in Fig. 1, the system consists of N distributed dynamic TXs, a single RX, and M moving targets. In this case, the positions and velocities of all TXs are assumed to be known, and the RX is fixed at the origin. In contrast, both the positions and velocities of the moving targets are unknown and must be estimated based on the received BR, BRR, and DOA measurements. All positions and motions are represented in spherical coordinates. Let $\mathcal{N} = \{1, 2, \ldots, N\}$ denote the index set of TXs. Each TX, denoted as the TX_n for all $n \in \mathcal{N}$, is positioned at $(r_n^{\mathrm{TX}}, \theta_n^{\mathrm{TX}}, \phi_n^{\mathrm{TX}})$, and moves with velocity $(v_{r,n}^{\mathrm{TX}}, v_{\theta,n}^{\mathrm{TX}}, v_{\phi,n}^{\mathrm{TX}})$. The collections of all TX positions and velocities are represented as:

$$\mathbf{TX}^{\mathrm{sph}} = [\mathbf{TX}_1, \mathbf{TX}_2, \ldots, \mathbf{TX}_N], \tag{1}$$

$$\dot{\mathbf{TX}}^{\mathrm{sph}} = [\dot{\mathbf{TX}}_1, \dot{\mathbf{TX}}_2, \ldots, \dot{\mathbf{TX}}_N], \tag{2}$$

where

$$\mathbf{TX}_n = [r_n^{\mathrm{TX}}, \theta_n^{\mathrm{TX}}, \phi_n^{\mathrm{TX}}]^T, \tag{3}$$

$$\dot{\mathbf{TX}}_n = [v_{r,n}^{\mathrm{TX}}, v_{\theta,n}^{\mathrm{TX}}, v_{\phi,n}^{\mathrm{TX}}]^T. \tag{4}$$

Similarly, let $\mathcal{M} = \{1, 2, \ldots, M\}$ denote the index set of targets. Each target, denoted as $\mathbf{A}_m$ for all $m \in \mathcal{M}$, is positioned at $(r_m^{\mathrm{A}}, \theta_m^{\mathrm{A}}, \phi_m^{\mathrm{A}})$, and moves with velocity $(v_{r,m}^{\mathrm{A}}, v_{\theta,m}^{\mathrm{A}}, v_{\phi,m}^{\mathrm{A}})$. The collections of all target positions and velocities are represented as:

$$\mathbf{A}^{\mathrm{sph}} = [\mathbf{A}_1, \mathbf{A}_2, \ldots, \mathbf{A}_M], \tag{5}$$

$$\dot{\mathbf{A}}^{\mathrm{sph}} = [\dot{\mathbf{A}}_1, \dot{\mathbf{A}}_2, \ldots, \dot{\mathbf{A}}_M], \tag{6}$$

where $\mathbf{A}_m = [r_m^{\mathrm{A}}, \theta_m^{\mathrm{A}}, \phi_m^{\mathrm{A}}]^T$ and $\dot{\mathbf{A}}_m = [v_{r,m}^{\mathrm{A}}, v_{\theta,m}^{\mathrm{A}}, v_{\phi,m}^{\mathrm{A}}]^T$.

1) Range Representation: Given the positions of the distributed TXs, RX, and targets, the range of the direct path between the TX_n and the RX, the range of the reflected path between the A_m and the RX, and the range of the target path between the TX_n and the A_m are expressed as follows:

$$d_n^{\mathrm{TX}} = r_n^{\mathrm{TX}}, \tag{7}$$

$$d_m^{\mathrm{A}} = r_m^{\mathrm{A}}, \tag{8}$$

$$d_{n,m}^{\mathrm{TX-A}} = \sqrt{(r_n^{\mathrm{TX}})^2 - 2 r_n^{\mathrm{TX}} r_m^{\mathrm{A}} \cos(\alpha_{n,m}) + (r_m^{\mathrm{A}})^2}, \tag{9}$$

where $\cos(\alpha_{n,m})$ represents the angular relationship between the TX_n and the A_m, and is given by

$$\begin{aligned}\cos(\alpha_{n,m}) = &\cos(\phi_n^{\mathrm{TX}})\cos(\phi_m^{\mathrm{A}}) \\ &+ \sin(\phi_n^{\mathrm{TX}})\sin(\phi_m^{\mathrm{A}})\cos(\theta_n^{\mathrm{TX}} - \theta_m^{\mathrm{A}}).\end{aligned} \tag{10}$$

Accordingly, the BR associated with the n-th TX-RX pair and the A_m is expressed as:

$$\Delta_{n,m}^{o} = d_{n,m}^{\mathrm{TX-A}} + d_m^{\mathrm{A}} - d_n^{\mathrm{TX}}. \tag{11}$$

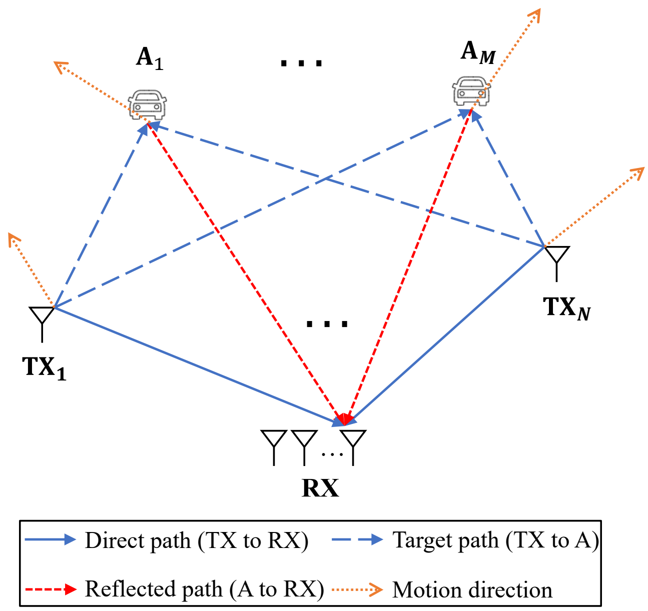

Fig. 1: The illustration of an ISAC system with M moving targets and N transmitters.

2) Range Rate Representation: Analogous to the range representation, given the velocities of the TXs and targets, the range rate of the direct path between the TX_n and the RX, and the range rate of the reflected path between the A_m and the RX can be expressed as follows:

$$\dot{d}_n^{\mathrm{TX}} = v_{r,n}^{\mathrm{TX}}, \tag{12}$$
$$\dot{d}_m^{\mathrm{A}} = v_{r,m}^{\mathrm{A}}. \tag{13}$$

The range rate of the target path between the TX_n and A_m is determined by the difference between their velocity projections onto the direction of the target path. To this end, the velocities of TX_n and A_m are first converted into global Cartesian coordinates as:

$$\dot{\mathbf{TX}}_n^{\mathrm{Car}} = v_{r,n}^{\mathrm{TX}}\hat{\mathbf{e}}_r^{\mathrm{TX}} + r_n^{\mathrm{TX}}\sin(\phi_n^{\mathrm{TX}})v_{\theta,n}^{\mathrm{TX}}\hat{\mathbf{e}}_\theta^{\mathrm{TX}} + r_n^{\mathrm{TX}}v_{\phi,n}^{\mathrm{TX}}\hat{\mathbf{e}}_\phi^{\mathrm{TX}}, \tag{14}$$
$$\dot{\mathbf{A}}_m^{\mathrm{Car}} = v_{r,m}^{\mathrm{A}}\hat{\mathbf{e}}_r^{\mathrm{A}} + r_m^{\mathrm{A}}\sin(\phi_m^{\mathrm{A}})v_{\theta,m}^{\mathrm{A}}\hat{\mathbf{e}}_\theta^{\mathrm{A}} + r_m^{\mathrm{A}}v_{\phi,m}^{\mathrm{A}}\hat{\mathbf{e}}_\phi^{\mathrm{A}}, \tag{15}$$

where the local spherical unit vectors $(\hat{\mathbf{e}}_r, \hat{\mathbf{e}}_\theta, \hat{\mathbf{e}}_\phi)$ are defined as:

$$\hat{\mathbf{e}}_r = [\sin(\phi)\cos(\theta),\ \sin(\phi)\sin(\theta),\ \cos(\phi)]^T, \tag{16}$$
$$\hat{\mathbf{e}}_\theta = [-\sin(\theta),\ \cos(\theta),\ 0]^T, \tag{17}$$
$$\hat{\mathbf{e}}_\phi = [\cos(\phi)\cos(\theta),\ \cos(\phi)\sin(\theta),\ -\sin(\phi)]^T. \tag{18}$$

The Cartesian coordinates of the TX_n and the A_m are given by:

$$\mathbf{TX}_n^{\mathrm{Car}} = r_n^{\mathrm{TX}}\begin{bmatrix}\sin(\phi_n^{\mathrm{TX}})\cos(\theta_n^{\mathrm{TX}})\\ \sin(\phi_n^{\mathrm{TX}})\sin(\theta_n^{\mathrm{TX}})\\ \cos(\phi_n^{\mathrm{TX}})\end{bmatrix}, \tag{19}$$
$$\mathbf{A}_m^{\mathrm{Car}} = r_m^{\mathrm{A}}\begin{bmatrix}\sin(\phi_m^{\mathrm{A}})\cos(\theta_m^{\mathrm{A}})\\ \sin(\phi_m^{\mathrm{A}})\sin(\theta_m^{\mathrm{A}})\\ \cos(\phi_m^{\mathrm{A}})\end{bmatrix}. \tag{20}$$

The unit direction vector from TX_n to A_m is computed as:

$$\hat{\mathbf{u}}_{n,m}^{\mathrm{TXA}} = \frac{\mathbf{TX}_n^{\mathrm{Car}} - \mathbf{A}_m^{\mathrm{Car}}}{\left\|\mathbf{TX}_n^{\mathrm{Car}} - \mathbf{A}_m^{\mathrm{Car}}\right\|}. \tag{21}$$

The projections of the velocities onto the path direction are then computed as:

$$v_{n,m}^{\mathrm{TX-TXA}} = \dot{\mathbf{TX}}_n^{\mathrm{Car}} \cdot \hat{\mathbf{u}}_{n,m}^{\mathrm{TXA}}, \tag{22}$$
$$v_{n,m}^{\mathrm{A-TXA}} = \dot{\mathbf{A}}_m^{\mathrm{Car}} \cdot \hat{\mathbf{u}}_{n,m}^{\mathrm{TXA}}. \tag{23}$$

Therefore, the range rate of the target path between the TX_n and the A_m is given by:

$$\dot{d}_{n,m}^{\mathrm{TXA}} = v_{n,m}^{\mathrm{TX-TXA}} - v_{n,m}^{\mathrm{A-TXA}}. \tag{24}$$

Accordingly, the BRR associated with the n-th TX-RX pair and the A_m is expressed as:

$$\dot{\Delta}_{n,m}^{o} = \dot{d}_{n,m}^{\mathrm{TXA}} + \dot{d}_m^{\mathrm{A}} - \dot{d}_n^{\mathrm{TX}}. \tag{25}$$

B. Model with Unknown-Location TXs

We next consider a multistatic sensing scenario for tracking multiple moving targets in an ISAC system with unknown-location TXs. The system configuration remains identical to that in Section II.A, except that the TXs are now static—i.e., their motion components in Fig. 1 are disregarded—and their positions are assumed to be unknown. Consequently, in addition to estimating the positions and velocities of the moving targets, the positions of all TXs must also be inferred from the received BR, BRR, and DOA measurements. The coordinate system remains consistent with that of Section II.A, but omits the TX velocity components.

1) Range Representation: Since the same coordinate system is adopted, the range expressions for the direct path between the TX_n and the RX, the reflected path between the A_m and the RX, and the target path between the TX_n and the A_m remain unchanged. Specifically, the range quantities d_n^{TX}, d_m^{A}, $d_{n,m}^{\mathrm{TX-A}}$, and $\Delta_{n,m}^{o}$ are still computed using equations (7)–(10).

2) Range Rate Representation: With static TXs, the direct path between the TX_n and the RX range rate becomes zero:

$$\dot{d}_n^{\mathrm{TX}} = 0. \tag{26}$$

The reflected path range rate between the A_m and the RX, $\dot{d}_m^{\mathrm{A}}$, remains as defined in (13), since the targets are still moving. Similarly, the range rate of the target path between the TX_n and target A_m can be derived by projecting the target velocity onto the target path direction. Following the same formulation in (15)–(21) and (23), the range rate of the target path between the TX_n and the A_m is given by:

$$\dot{d}_{n,m}^{\mathrm{TXA}} = v_{n,m}^{\mathrm{A-TXA}}. \tag{27}$$

Accordingly, the BRR associated with the n-th TX-RX pair and the A_m is updated as:

$$\dot{\Delta}_{n,m}^{o} = \dot{d}_{n,m}^{\mathrm{TXA}} + \dot{d}_m^{\mathrm{A}}. \tag{28}$$

C. Measurement Model with Noise

As described earlier, three types of measurements are acquired at the RX: BR, BRR, and DOA. In the 3D model, each DOA measurement includes both azimuth and elevation components. Although our focus is on the geometric estimation stage after obtaining the BR, BRR, and DOA measurements, these measurements are not perfectly accurate in practice. They can be affected by factors such as sidelobe interference, multipath propagation in complex environments, hardware impairments including phase noise and frequency instability, and array imperfections that limit angular resolution [42]–[44]. To capture these effects in a tractable manner, we model the observations as the sum of their true values and additive zero-mean Gaussian noise, which provides a unified abstraction of these practical uncertainties. For the model with dynamic TXs, the measured BR, BRR, azimuth DOA, and elevation DOA associated with the n-th TX-RX pair and the target A_m are given by:

$$\Delta_{n,m} = \Delta^o_{n,m} + w_{n,m}, \tag{29}$$

$$\dot{\Delta}_{n,m} = \dot{\Delta}^o_{n,m} + \dot{w}_{n,m}, \tag{30}$$

$$\beta^{\mathrm{A}}_{n,m} = \theta^{\mathrm{A}}_m + w^{\mathrm{Azi}}_{n,m}, \tag{31}$$

$$\psi^{\mathrm{A}}_{n,m} = \phi^{\mathrm{A}}_m + w^{\mathrm{Ele}}_{n,m}, \tag{32}$$

where $w_{n,m}$, $\dot{w}_{n,m}$, $w^{\mathrm{Azi}}_{n,m}$, and $w^{\mathrm{Ele}}_{n,m}$ are independent zero-mean Gaussian noise terms with variances σ^2_{BR}, σ^2_{BRR}, σ^2_1, and σ^2_2, respectively.

In the case of unknown-location TXs, the RX also measures the azimuth and elevation DOAs of each TX_n via the direct path:

$$\beta^{\mathrm{TX}}_n = \theta^{\mathrm{TX}}_n + \tilde{w}^{\mathrm{Azi}}_n, \tag{33}$$

$$\psi^{\mathrm{TX}}_n = \phi^{\mathrm{TX}}_n + \tilde{w}^{\mathrm{Ele}}_n, \tag{34}$$

where $\tilde{w}^{\mathrm{Azi}}_n$ and $\tilde{w}^{\mathrm{Ele}}_n$ are also additive zero-mean Gaussian noises with variances σ^2_3 and σ^2_4, respectively. For simplicity, all angle measurement variances are assumed equal and denoted by σ^2_{DOA}, i.e., $\sigma^2_1 = \sigma^2_2 = \sigma^2_3 = \sigma^2_4 = \sigma^2_{\mathrm{DOA}}$.

Consequently, in a system with *N* TX-RX pairs and *M* targets, a total of *NM* BR, BRR, azimuth, and elevation DOA measurements are obtained. For the case of unknown-location TXs, *N* additional azimuth and elevation DOA measurements are also collected. The first objective of this paper is to determine the position and velocity of each target based on the noisy measurements under the model with dynamic TXs. The second objective is to jointly estimate the positions of the TXs, as well as the positions and velocities of the targets, based on the noisy measurements in the ISAC system with unknown-location TXs.

D. Per-Target Decomposition

As described in the previous subsections, the RX acquires a set of measurements from both the direct path and the reflected path associated with each TX-RX-Target triplet [20]. Specifically, for each TX-RX pair and target, the RX obtains: (i) the DOAs of the TX_n, β^{TX}_n and ψ^{TX}_n, via the direct path, (ii) the BR $\Delta_{n,m}$ and BRR $\dot{\Delta}_{n,m}$, and (iii) the DOAs of the target, β^{A}_n and ψ^{A}_n, via the reflected path. These six measurements are jointly derived from the same pair of signal paths (direct and reflected) [20], and thus form one coherent measurement group.

In the dynamic TX scenario, where the positions and velocities of TXs are known, the DOAs β^{TX}_n and ψ^{TX}_n become redundant and are not required for estimation. With *N* TX-RX pairs and *M* targets, the RX acquires *NM* such measurement groups—each corresponding to one TX-RX-target configuration and consisting of $\{\Delta_{n,m}, \dot{\Delta}_{n,m}, \beta^{\mathrm{TX}}_n, \psi^{\mathrm{TX}}_n, \beta^{\mathrm{A}}_n, \psi^{\mathrm{A}}_n\}$. It is important to emphasize that these measurements are acquired in a structured, group-wise fashion at the sensing front-end. There is no mixing of signals across triplets, ensuring that each measurement group remains independent and traceable.

To enable scalable multi-target localization, we make a key assumption: all targets are spatially separable in the angular domain. That is, their reflected DOAs are sufficiently distinct such that the RX can associate each group of measurements with the correct target, even in the presence of moderate DOA noise. Under this assumption, the RX can partition the *NM* measurement groups into *M* non-overlapping sets, each associated with a single target and its corresponding *N* TX-RX pairs. This structure allows the multi-target localization problem to be decomposed into *M* independent subproblems, each solvable using the same estimation procedure. For clarity, the remainder of this paper focuses on the single-target case; extension to multiple targets is via repeated application of the proposed method to each measurement cluster.

We acknowledge that in dense environments or when targets are closely spaced in angle, the assumption of angular separability may not hold. In such cases, reliable measurement association becomes a nontrivial challenge, necessitating additional signal processing techniques, such as joint DOA-delay clustering, probabilistic data association, or Bayesian inference. These directions, while beyond the scope of this work, form an important avenue for future research aimed at enabling robust multi-target tracking in practical ISAC deployments.

III. Localization Algorithm

In this section, two localization algorithms are developed based on the BR, BRR, and DOA measurements introduced in Section II. Section III.A presents an algorithm tailored for the case with dynamic TXs, where the positions and velocities of all TXs are known to the RX. Section III.B addresses the scenario where the TX positions are unknown and must be jointly estimated along with the target states. All proposed algorithms are formulated on a per-target basis. That is, the estimation is performed for one target at a time using its associated measurements. As discussed in Section II.D, since the measurements corresponding to different targets are independent, the multi-target localization problem can be decomposed into a set of parallel single-target estimation tasks. Therefore, the proposed algorithms can be directly extended to the multi-target case by applying them to each target individually.

We denote the estimated A_m position and velocity in spherical coordinates as $(\bar{r}_m^{\mathrm{A}}, \bar{\theta}_m^{\mathrm{A}}, \bar{\phi}_m^{\mathrm{A}})$ and $(\bar{v}_{r,m}^{\mathrm{A}}, \bar{v}_{\theta,m}^{\mathrm{A}}, \bar{v}_{\phi,m}^{\mathrm{A}})$, respectively.

A. Localization with Dynamic TXs

1) Position Estimation: Based on the previously defined measurements $\Delta_{n,m}$, $\beta_{n,m}^{\mathrm{A}}$, and $\psi_{n,m}^{\mathrm{A}}$, we construct the following measurement vectors:

$$\mathbf{\Delta}_m = [\Delta_{1,m}, \Delta_{2,m}, \ldots, \Delta_{N,m}]^T, \tag{35}$$

$$\boldsymbol{B}_m^{\mathrm{A}} = [\beta_{1,m}^{\mathrm{A}}, \beta_{2,m}^{\mathrm{A}}, \ldots, \beta_{N,m}^{\mathrm{A}}]^T, \tag{36}$$

$$\mathbf{\Psi}_m^{\mathrm{A}} = [\psi_{1,m}^{\mathrm{A}}, \psi_{2,m}^{\mathrm{A}}, \ldots, \psi_{N,m}^{\mathrm{A}}]^T. \tag{37}$$

The target's azimuth and elevation angles are estimated by minimizing the discrepancy between the observed DOA vectors and ideal constant vectors:

$$\bar{\theta}_m^{\mathrm{A}} = \arg \min_{\bar{\theta}_m^{\mathrm{A}} \in [0,2\pi]} \|\bar{\theta}_m^{\mathrm{A}} \mathbf{1}_N - \boldsymbol{B}_m^{\mathrm{A}}\|, \tag{38}$$

$$\bar{\phi}_m^{\mathrm{A}} = \arg \min_{\bar{\phi}_m^{\mathrm{A}} \in [0,\pi]} \|\bar{\phi}_m^{\mathrm{A}} \mathbf{1}_N - \mathbf{\Psi}_m^{\mathrm{A}}\|. \tag{39}$$

Next, by substituting (7)–(10) into (11), the true BR $\Delta_{n,m}^o$ can be expressed as:

$$\Delta_{n,m}^o = \sqrt{(r_n^{\mathrm{TX}})^2 - 2 r_n^{\mathrm{TX}} r_m^{\mathrm{A}} \cos(\alpha_{n,m}) + (r_m^{\mathrm{A}})^2} + r_m^{\mathrm{A}} - r_n^{\mathrm{TX}}, \tag{40}$$

where

$$\begin{aligned}\cos(\alpha_{n,m}) = &\sin(\phi_n^{\mathrm{TX}}) \sin(\phi_m^{\mathrm{A}}) \cos(\theta_n^{\mathrm{TX}} - \theta_m^{\mathrm{A}}) \\ &+ \cos(\phi_n^{\mathrm{TX}}) \cos(\phi_m^{\mathrm{A}}).\end{aligned} \tag{41}$$

Since the target's position is unknown, we estimate the range $\bar{r}_m^{\mathrm{A}}$, azimuth $\bar{\theta}_m^{\mathrm{A}}$, and elevation $\bar{\phi}_m^{\mathrm{A}}$ by solving for their estimated values. The estimated BR is then expressed as:

$$\bar{\Delta}_{n,m} = \sqrt{(r_n^{\mathrm{TX}})^2 - 2 r_n^{\mathrm{TX}} \bar{r}_m^{\mathrm{A}} \cos(\bar{\alpha}_{n,m}) + (\bar{r}_m^{\mathrm{A}})^2} + \bar{r}_m^{\mathrm{A}} - r_n^{\mathrm{TX}}, \tag{42}$$

where

$$\begin{aligned}\cos(\bar{\alpha}_{n,m}) = &\sin(\phi_n^{\mathrm{TX}}) \sin(\bar{\phi}_m^{\mathrm{A}}) \cos(\theta_n^{\mathrm{TX}} - \bar{\theta}_m^{\mathrm{A}}) \\ &+ \cos(\phi_n^{\mathrm{TX}}) \cos(\bar{\phi}_m^{\mathrm{A}}).\end{aligned} \tag{43}$$

By stacking the estimated BRs for all N TX–RX pairs, we define:

$$\bar{\mathbf{\Delta}}_m = [\bar{\Delta}_{1,m}, \bar{\Delta}_{2,m}, \ldots, \bar{\Delta}_{N,m}]^T. \tag{44}$$

The optimal target range $\bar{r}_m^{\mathrm{A}}$ is then estimated by minimizing the mismatch between the estimated and measured BR vectors:

$$\bar{r}_m^{\mathrm{A}} = \arg \min_{\bar{r}_m^{\mathrm{A}} \in [0,R]} \|\bar{\mathbf{\Delta}}_m - \mathbf{\Delta}_m\|, \tag{45}$$

where R is the predefined maximum search range.

By solving (38), (39), and (45) based on the maximum likelihood principle, the 3D position of the target can be estimated. It is worth noting that the number of optimization variables is only one in each of those steps, which implies that the position can be estimated with only one TX–RX pair (i.e., $N = 1$).

2) Velocity Estimation: Similarly, based on the previously defined measurements $\dot{\Delta}_{n,m}$, we construct the following measurement vector:

$$\dot{\mathbf{\Delta}}_m = [\dot{\Delta}_{1,m}, \dot{\Delta}_{2,m}, \ldots, \dot{\Delta}_{N,m}]^T. \tag{46}$$

By substituting (12)–(24) into (25), the true BRR $\dot{\Delta}_{n,m}^o$ can be expressed as:

$$\dot{\Delta}_{n,m}^o = \dot{\mathbf{TX}}_n^{\mathrm{Car}} \cdot \hat{\mathbf{u}}_{n,m}^{\mathrm{TXA}} - \dot{\mathbf{A}}_m^{\mathrm{Car}} \cdot \hat{\mathbf{u}}_{n,m}^{\mathrm{TXA}} + v_{r,m}^{\mathrm{A}} - v_{r,n}^{\mathrm{TX}}, \tag{47}$$

where

$$\hat{\mathbf{u}}_{n,m}^{\mathrm{TXA}} = \frac{\mathbf{TX}_n^{\mathrm{Car}} - \mathbf{A}_m^{\mathrm{Car}}}{\left\| \mathbf{TX}_n^{\mathrm{Car}} - \mathbf{A}_m^{\mathrm{Car}} \right\|}. \tag{48}$$

Since the target velocity is unknown, we estimate the range rate $v_{r,m}^{\mathrm{A}}$, azimuth rate $v_{\theta,m}^{\mathrm{A}}$, and elevation rate $v_{\phi,m}^{\mathrm{A}}$ by solving for their estimates $\bar{v}_{r,m}^{\mathrm{A}}$, $\bar{v}_{\theta,m}^{\mathrm{A}}$, and $\bar{v}_{\phi,m}^{\mathrm{A}}$. The target position is estimated as:

$$\bar{\mathbf{A}}_m = [\bar{r}_m^{\mathrm{A}}, \bar{\theta}_m^{\mathrm{A}}, \bar{\phi}_m^{\mathrm{A}}]^T. \tag{49}$$

The estimated position and velocity in global Cartesian coordinates are expressed as:

$$\bar{\mathbf{A}}_m^{\mathrm{Car}} = \bar{r}_m^{\mathrm{A}} \begin{bmatrix} \sin(\bar{\phi}_m^{\mathrm{A}}) \cos(\bar{\theta}_m^{\mathrm{A}}) \\ \sin(\bar{\phi}_m^{\mathrm{A}}) \sin(\bar{\theta}_m^{\mathrm{A}}) \\ \cos(\bar{\phi}_m^{\mathrm{A}}) \end{bmatrix}, \tag{50}$$

$$\dot{\mathbf{A}}_m^{\mathrm{Car}} = \bar{v}_{r,m}^{\mathrm{A}} \hat{\mathbf{e}}_r^{\mathrm{A}} + \bar{r}_m^{\mathrm{A}} \sin(\bar{\phi}_m^{\mathrm{A}})\, \bar{v}_{\theta,m}^{\mathrm{A}} \hat{\mathbf{e}}_\theta^{\mathrm{A}} + \bar{r}_m^{\mathrm{A}} \bar{v}_{\phi,m}^{\mathrm{A}} \hat{\mathbf{e}}_\phi^{\mathrm{A}}, \tag{51}$$

where the spherical unit vectors are given by:

$$\hat{\mathbf{e}}_r^{\mathrm{A}} = \begin{bmatrix} \sin(\bar{\phi}_m^{\mathrm{A}}) \cos(\bar{\theta}_m^{\mathrm{A}}) \\ \sin(\bar{\phi}_m^{\mathrm{A}}) \sin(\bar{\theta}_m^{\mathrm{A}}) \\ \cos(\bar{\phi}_m^{\mathrm{A}}) \end{bmatrix}, \tag{52}$$

$$\hat{\mathbf{e}}_\theta^{\mathrm{A}} = \begin{bmatrix} -\sin(\bar{\theta}_m^{\mathrm{A}}) \\ \cos(\bar{\theta}_m^{\mathrm{A}}) \\ 0 \end{bmatrix}, \tag{53}$$

$$\hat{\mathbf{e}}_\phi^{\mathrm{A}} = \begin{bmatrix} \cos(\bar{\phi}_m^{\mathrm{A}}) \cos(\bar{\theta}_m^{\mathrm{A}}) \\ \cos(\bar{\phi}_m^{\mathrm{A}}) \sin(\bar{\theta}_m^{\mathrm{A}}) \\ -\sin(\bar{\phi}_m^{\mathrm{A}}) \end{bmatrix}. \tag{54}$$

The estimated BRR is then expressed as:

$$\bar{\Delta}_{n,m} = \dot{\mathbf{TX}}_n^{\mathrm{Car}} \cdot \hat{\mathbf{u}}_{n,m}^{\mathrm{TXA}} - \dot{\mathbf{A}}_m^{\mathrm{Car}} \cdot \hat{\mathbf{u}}_{n,m}^{\mathrm{TXA}} + \bar{v}_{r,m}^{\mathrm{A}} - v_{r,n}^{\mathrm{TX}}. \tag{55}$$

By stacking the estimated BRRs for all N TX–RX pairs, we define:

$$\bar{\mathbf{\Delta}}_m = [\bar{\Delta}_{1,m}, \bar{\Delta}_{2,m}, \ldots, \bar{\Delta}_{N,m}]^T. \tag{56}$$

The optimal target velocity is then estimated by minimizing the mismatch between estimated and measured BRR vectors:

$$(\bar{v}_{r,m}^{\mathrm{A}}, \bar{v}_{\theta,m}^{\mathrm{A}}, \bar{v}_{\phi,m}^{\mathrm{A}}) = \arg \min_{\substack{\bar{v}_{r,m}^{\mathrm{A}} \in [0,V_r], \\ \bar{v}_{\theta,m}^{\mathrm{A}} \in [0,V_\theta], \\ \bar{v}_{\phi,m}^{\mathrm{A}} \in [0,V_\phi]}} \left\| \bar{\mathbf{\Delta}}_m - \dot{\mathbf{\Delta}}_m \right\|, \tag{57}$$

where V_r, V_θ, and V_ϕ are predefined search ranges.

3) Computational Complexity Analysis: The proposed algorithm estimates the target range, azimuth, and elevation angles each via independent one-dimensional searches in (38), (39), and (45). Accordingly, the computational complexity for the position estimation of a single target is:

$$\mathcal{O}\big(N(R_{\max} + \Theta^{\mathrm{A}}_{\max} + \Phi^{\mathrm{A}}_{\max})\big)\,, \tag{58}$$

where $R_{\max}$, $\Theta^{\mathrm{A}}_{\max}$, and $\Phi^{\mathrm{A}}_{\max}$ denote the number of search steps. For M independent targets, the complexity scales linearly as:

$$\mathcal{O}\big(NM(R_{\max} + \Theta^{\mathrm{A}}_{\max} + \Phi^{\mathrm{A}}_{\max})\big)\,. \tag{59}$$

In addition, velocity estimation requires a 3D grid search in (57), building upon the prior position estimate. The complexity becomes:

$$\mathcal{O}\big(N(R_{\max} + \Theta^{\mathrm{A}}_{\max} + \Phi^{\mathrm{A}}_{\max} + V_{r,\max}V_{\theta,\max}V_{\phi,\max})\big)\,, \tag{60}$$

and for M targets:

$$\mathcal{O}\big(NM(R_{\max} + \Theta^{\mathrm{A}}_{\max} + \Phi^{\mathrm{A}}_{\max} + V_{r,\max}V_{\theta,\max}V_{\phi,\max})\big)\,. \tag{61}$$

B. Localization with Unknown-Location TXs

1) Localization: Although this section addresses a different scenario, it still shares several settings with Section III.A, and some equations can be reused accordingly. In addition to the measurement vectors defined in (35)–(37) and (44), the RX can also measure the azimuth and elevation DOAs of each TX_n when the TX positions are unknown. Based on the previously defined measurements β^{TX}_n and ψ^{TX}_n, we construct the following measurement vectors:

$$\boldsymbol{B}^{\mathrm{TX}} = [\beta^{\mathrm{TX}}_1, \beta^{\mathrm{TX}}_2, \ldots, \beta^{\mathrm{TX}}_N]^T, \tag{62}$$

$$\boldsymbol{\Psi}^{\mathrm{TX}} = [\psi^{\mathrm{TX}}_1, \psi^{\mathrm{TX}}_2, \ldots, \psi^{\mathrm{TX}}_N]^T. \tag{63}$$

We denote the estimated TX_n position in spherical coordinates as $[r^{\mathrm{TX}}_n, \theta^{\mathrm{TX}}_n, \phi^{\mathrm{TX}}_n]^T$. Since both the positions of TXs and the target's position and velocity are unknown, we jointly estimate the position of the TX_n, the position and velocity of the A_m. This is done by solving for their corresponding estimates: $\bar{r}^{\mathrm{TX}}_n, \bar{\theta}^{\mathrm{TX}}_n, \bar{\phi}^{\mathrm{TX}}_n, \bar{r}^{\mathrm{A}}_m, \bar{\theta}^{\mathrm{A}}_m, \bar{\phi}^{\mathrm{A}}_m, \bar{v}^{\mathrm{A}}_{r,m}, \bar{v}^{\mathrm{A}}_{\theta,m}, \bar{v}^{\mathrm{A}}_{\phi,m}$.

The measured azimuth and elevation DOAs of TXs are directly taken as their estimates, i.e., $\bar{\theta}^{\mathrm{TX}}_n = \beta^{\mathrm{TX}}_n$ and $\bar{\phi}^{\mathrm{TX}}_n = \psi^{\mathrm{TX}}_n$. The target's azimuth and elevation angles are estimated using the same method in (38) and (39).

The estimated BR in (42) is now updated as:

$$\bar{\Delta}_{n,m} = \sqrt{(r^{\mathrm{TX}}_n)^2 - 2r^{\mathrm{TX}}_n\bar{r}^{\mathrm{A}}_m\cos(\bar{\alpha}_{n,m}) + (\bar{r}^{\mathrm{A}}_m)^2} + \bar{r}^{\mathrm{A}}_m - r^{\mathrm{TX}}_n, \tag{64}$$

where

$$\cos(\bar{\alpha}_{n,m}) = \sin(\phi^{\mathrm{TX}}_n)\sin(\bar{\phi}^{\mathrm{A}}_m)\cos(\theta^{\mathrm{TX}}_n - \bar{\theta}^{\mathrm{A}}_m) + \cos(\phi^{\mathrm{TX}}_n)\cos(\bar{\phi}^{\mathrm{A}}_m). \tag{65}$$

Rearranging (64) and squaring both sides, we obtain an expression for r^{TX}_n as:

$$r^{\mathrm{TX}}_n = \frac{(\Delta_{n,m})^2 - 2\bar{r}^{\mathrm{A}}_m\bar{\Delta}_{n,m}}{2\bar{r}^{\mathrm{A}}_m - 2\bar{r}^{\mathrm{A}}_m\cos(\bar{\alpha}_{n,m})}. \tag{66}$$

By taking measured BR as the estimated BR, i.e., $\bar{\Delta}_{n,m} = \Delta_{n,m}$, each r^{TX}_n can be estimated once $\bar{r}^{\mathrm{A}}_m$ is obtained.

Substituting (13), (15)–(21), (23), (26), and (27) into (28), the true BRR is expressed as:

$$\dot{\Delta}^o_{n,m} = \dot{\mathbf{TX}}^{\mathrm{Car}}_n \cdot \hat{\mathbf{u}}^{\mathrm{TXA}}_{n,m} - \dot{\mathbf{A}}^{\mathrm{Car}}_m \cdot \hat{\mathbf{u}}^{\mathrm{TXA}}_{n,m} + v^{\mathrm{A}}_{r,m} - v^{\mathrm{TX}}_{r,n}, \tag{67}$$

where

$$\hat{\mathbf{u}}^{\mathrm{TXA}}_{n,m} = \frac{\mathbf{TX}^{\mathrm{Car}}_n - \mathbf{A}^{\mathrm{Car}}_m}{\left\|\mathbf{TX}^{\mathrm{Car}}_n - \mathbf{A}^{\mathrm{Car}}_m\right\|}. \tag{68}$$

The estimated position of TX_n in global Cartesian coordinates is expressed as:

$$\mathbf{TX}^{\mathrm{Car}}_n = r^{\mathrm{TX}}_n \begin{bmatrix} \sin(\theta^{\mathrm{TX}}_n)\cos(\phi^{\mathrm{TX}}_n) \\ \sin(\theta^{\mathrm{TX}}_n)\sin(\phi^{\mathrm{TX}}_n) \\ \cos(\phi^{\mathrm{TX}}_n) \end{bmatrix}. \tag{69}$$

The estimated position and velocity of A_m are expressed in (50) and (51). The estimated BRR is then given by:

$$\bar{\Delta}_{n,m} = \dot{\mathbf{TX}}^{\mathrm{Car}}_n \cdot \hat{\mathbf{u}}^{\mathrm{TXA}}_{n,m} - \dot{\mathbf{A}}^{\mathrm{Car}}_m \cdot \hat{\mathbf{u}}^{\mathrm{TXA}}_{n,m} + \bar{v}^{\mathrm{A}}_{r,m} - v^{\mathrm{TX}}_{r,n}. \tag{70}$$

By stacking all estimated BRRs for all N TX–RX pairs, we define:

$$\bar{\boldsymbol{\Delta}}_m = [\bar{\Delta}_{1,m}, \bar{\Delta}_{2,m}, \ldots, \bar{\Delta}_{N,m}]^T. \tag{71}$$

The optimal target range $\bar{r}^{\mathrm{A}}_m$ and velocity parameters are jointly estimated by minimizing:

$$(\bar{r}^{\mathrm{A}}_m, \bar{v}^{\mathrm{A}}_{r,m}, \bar{v}^{\mathrm{A}}_{\theta,m}, \bar{v}^{\mathrm{A}}_{\phi,m}) = \arg \min_{\substack{\bar{r}^{\mathrm{A}}_m \in [0,R],\\ \bar{v}^{\mathrm{A}}_{r,m} \in [0,V_r],\\ \bar{v}^{\mathrm{A}}_{\theta,m} \in [0,V_\theta],\\ \bar{v}^{\mathrm{A}}_{\phi,m} \in [0,V_\phi]}} \left\|\bar{\boldsymbol{\Delta}}_m - \dot{\boldsymbol{\Delta}}_m\right\|. \tag{72}$$

By solving (72) based on the maximum likelihood principle, the 3D position and velocity of the target can be estimated. The positions of the TXs are determined using (66). In this case, the total number of optimization variables is four. Thus, at least four TX–RX pairs (i.e., $N = 4$) are required to perform the estimation in principle.

2) Computational Complexity Analysis: The proposed algorithm first estimates the azimuth and elevation angles of the target using independent 1D searches in (38) and (39). Subsequently, the target's range and velocity are jointly estimated through a four-dimensional (4D) grid search. The positions of the TXs are simultaneously obtained in this process. Accordingly, the computational complexity for localizing a single target is:

$$\mathcal{O}\big(N(\Theta^{\mathrm{A}}_{\max} + \Phi^{\mathrm{A}}_{\max} + R_{\max} + V_{r,\max}V_{\theta,\max}V_{\phi,\max})\big)\,, \tag{73}$$

and for M targets the complexity becomes:

$$\mathcal{O}\big(NM(\Theta^{\mathrm{A}}_{\max} + \Phi^{\mathrm{A}}_{\max} + R_{\max} + V_{r,\max}V_{\theta,\max}V_{\phi,\max})\big)\,. \tag{74}$$

TABLE I: Positions of the TXs and the RX

System	(r, θ, ϕ)
RX	$(0, 0, 0)$
TX_1	$(50, 15, 20)$
TX_2	$(20, 20, 10)$
TX_3	$(25, 15, 15)$
TX_4	$(40, 5, 45)$

TABLE II: Velocities of the TXs

System	(v_r, v_θ, v_ϕ)
TX_1	(3, 0.5, 1)
TX_2	(2, 1, 1)
TX_3	(1.5, 1.5, 0.5)
TX_4	(1, 0.7, 0.5)

IV. Simulations

In this section, we present simulation results to evaluate the performance of the proposed localization algorithms. We consider an ISAC system consisting of a single static RX equipped with an antenna array and four TXs, with the goal of estimating the position and velocity of an unknown moving target. The positions of the TXs and the RX are listed in Table I, and the velocities of the TXs are provided in Table II. The units of range, range rate, angle, and angular rate used in simulations are meter (m), meter per second (m/s), degree (°), and degree per second (°/s), respectively.

In Section IV.A, the TXs are assumed to be dynamic, and both the positional and velocity information from Tables I and II are used in the simulations. The proposed algorithm is compared against an existing localization method for dynamic TXs introduced in [24], which we refer to as the two-stage weighted least squares (2WLS) method for brevity.

In Section IV.B, the TXs are assumed to be static, and only the positional information from Table I is used. The proposed algorithm is compared with a method introduced in [24] for localizing a moving target using static TXs with known positions. This comparison demonstrates the capability of the proposed method to simultaneously localize both the target and the TXs when the TX positions are unknown. To better evaluate the performance, the estimation results are converted from spherical to Cartesian coordinates. The RMSEs of the estimated target position and velocity in Cartesian coordinates are defined as:

$$\text{RMSE}_{\text{position}} = \sqrt{\frac{1}{L}\sum_{l=1}^{L}\left\|\mathbf{A}_m^{\text{Car}} - \hat{\mathbf{A}}_{l,m}^{\text{Car}}\right\|^2}, \tag{75}$$

$$\text{RMSE}_{\text{velocity}} = \sqrt{\frac{1}{L}\sum_{l=1}^{L}\left\|\dot{\mathbf{A}}_m^{\text{Car}} - \hat{\dot{\mathbf{A}}}_{l,m}^{\text{Car}}\right\|^2}, \tag{76}$$

where $\mathbf{A}_m^{\text{Car}}$ and $\dot{\mathbf{A}}_m^{\text{Car}}$ denote the ground-truth position and velocity of the target A_m, and $\hat{\mathbf{A}}_{l,m}^{\text{Car}}$ and $\hat{\dot{\mathbf{A}}}_{l,m}^{\text{Car}}$ are the corresponding estimates obtained in the l-th Monte Carlo trial. Each experiment is repeated over 5000 independent trials.

As described in Section II.C, zero-mean Gaussian noises are added to the BR, BRR, and DOA measurements in each trial. The noisy BR and BRR measurements $\Delta_{n,m}$ and $\dot{\Delta}_{n,m}$ have noise variances σ_{BR}^2 and σ_{BRR}^2, respectively, while the noisy azimuth and elevation DOAs $\beta_{n,m}^{\text{A}}$, $\psi_{n,m}^{\text{A}}$, β_n^{TX}, and ψ_n^{TX} have noise variance σ_{DOA}^2. The target is positioned at $(50, 90, 75)$ with a velocity of $(20, 1, 5)$ in spherical coordinates. Unless stated otherwise, the proposed algorithm employs exhaustive grid search. The step sizes for range, angle, range rate, and angular rate are set to 0.01 m, 0.01°, 0.01 m/s, and 0.01°/s, respectively.

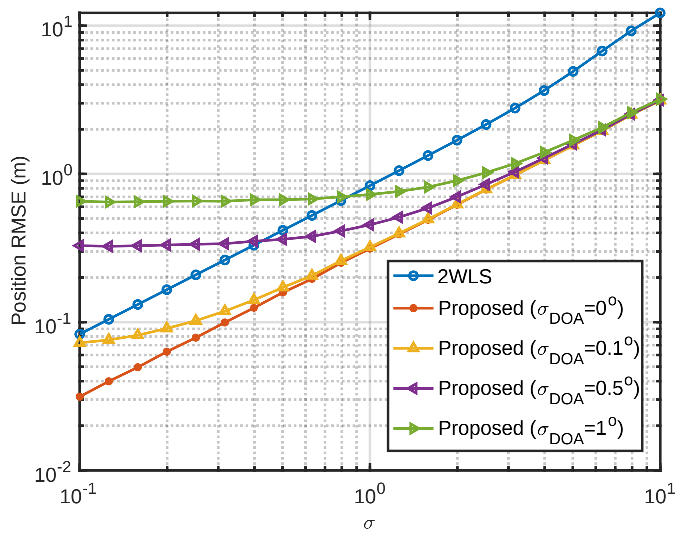

Fig. 2: Position RMSE comparison (3 TX-RX pairs).

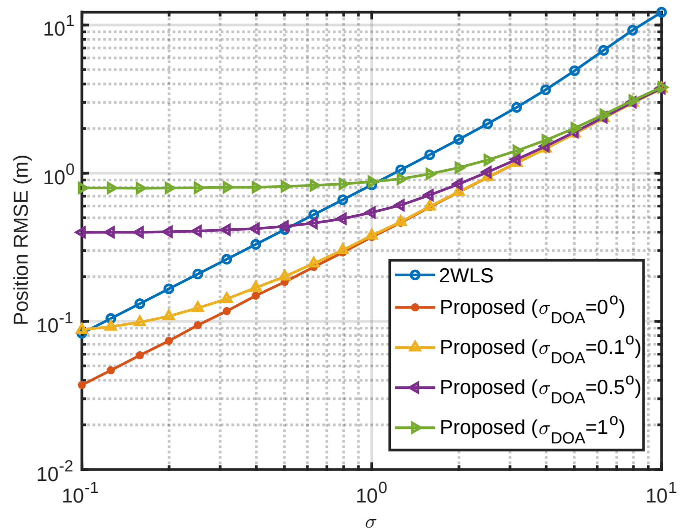

Fig. 3: Position RMSE comparison (2 TX-RX pairs).

A. Performance with Dynamic TXs

Only noisy $\Delta_{n,m}$, $\dot{\Delta}_{n,m}$, $\beta_{n,m}^{\text{A}}$, and $\psi_{n,m}^{\text{A}}$ measurements are used in this case and $N = 3$. Given that DOA measurements are not utilized in the 2WLS, we perform simulations of our proposed method by considering different levels of DOA noise, $\sigma_{\text{DOA}} \in \{0°, 0.1°, 0.5°, 1°\}$. We then compare our proposed method with these settings to 2WLS under the same noise standard deviations σ_{BR} and σ_{BRR}. Without loss of generality, we set a unitless variable σ, where $\sigma_{\text{BR}} = \sigma$ and $\sigma_{\text{BRR}} = 0.1\sigma$.

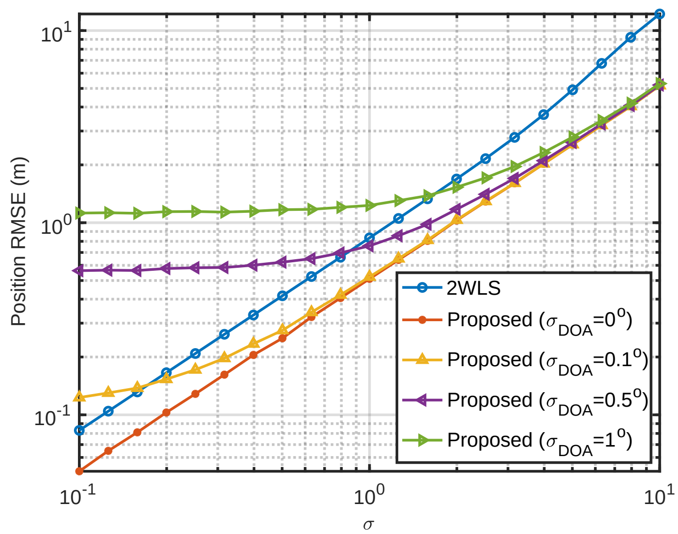

Fig. 4: Position RMSE comparison (1 TX-RX pair).

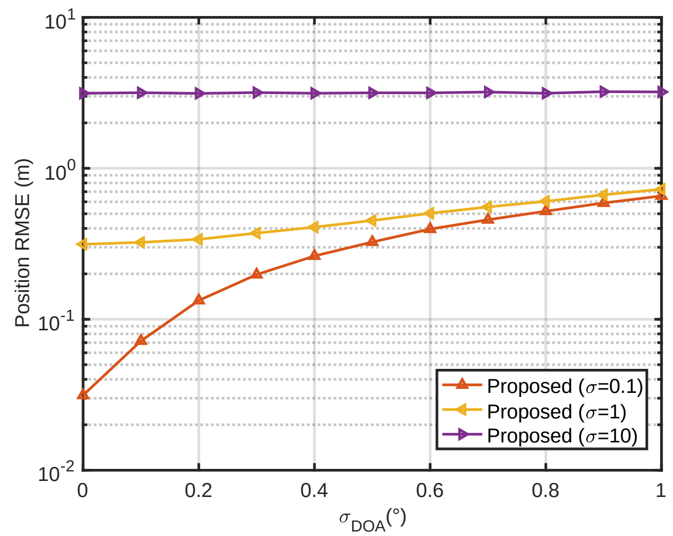

Fig. 6: Position RMSE comparison (angle).

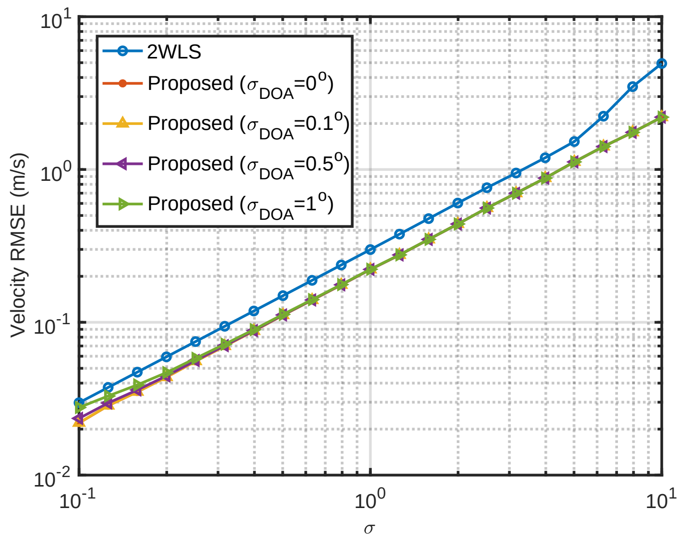

Fig. 5: Velocity RMSE comparison.

We first evaluate the position estimation performance of the proposed method and the 2WLS benchmark under varying noise conditions. Fig. 2 illustrates the position RMSEs with 3 TX–RX pairs as σ increases from 10^{-1} to 10^{1}. The results show that the proposed method significantly outperforms 2WLS in low-to-moderate DOA noise settings. Specifically, for $\sigma_{\mathrm{DOA}} = 0°$ and $\sigma_{\mathrm{DOA}} = 0.1°$, the proposed method yields much lower RMSEs across the entire range of σ, demonstrating strong robustness to BR and BRR noise. In contrast, when the DOA noise increases to $0.5°$ and $1°$, the performance of the proposed method degrades, particularly in the low-noise regime ($\sigma < 1$). In these cases, 2WLS exhibits slightly better position estimation accuracy. However, as σ continues to increase beyond 1, the proposed method becomes more resilient and ultimately surpasses 2WLS in high-noise conditions.

Figs. 3 and 4 present the position RMSEs under the same noise conditions but with reduced numbers of TX–RX pairs (2 and 1, respectively). A consistent trend is observed across all configurations: the performance of both methods degrades as the number of TX–RX pairs decreases, with RMSEs increasing more rapidly for all cases. This highlights the importance of measurement diversity in multistatic sensing. Notably, the proposed method maintains its advantage over 2WLS at low σ_{DOA} even with fewer TX–RX pairs, although the margin decreases. For higher DOA noise levels, the performance gap narrows significantly, and the benefits of the proposed method become less prominent, particularly in the single TX–RX case where geometric ambiguity increases.

These results collectively demonstrate that while the proposed method is more accurate under favorable DOA conditions, its relative advantage diminishes when the number of TX–RX pairs or the angular measurement accuracy is limited.

Next, Fig. 5 illustrates the velocity RMSEs of the proposed method and the 2WLS benchmark under varying noise levels σ, evaluated using 3 TX–RX pairs. As σ increases logarithmically from 10^{-1} to 10^{1}, both methods exhibit increasing velocity estimation error. However, the proposed method consistently achieves lower RMSEs than 2WLS across all σ values. Notably, the impact of DOA noise on the velocity estimation accuracy is minimal. The curves corresponding to different σ_{DOA} levels ($0°$, $0.1°$, $0.5°$, and $1°$) are nearly indistinguishable for the proposed method, suggesting that velocity estimation is primarily governed by the BRR measurements rather than the angular information. This observation aligns with the formulation in Section III, where the velocity components are estimated based on range-rate information that is less sensitive to DOA errors.

These results validate the robustness of the proposed approach in velocity estimation, even under challenging noise conditions and imperfect angular measurements.

To further investigate the effect of DOA noise, we analyze the performance over varying $\sigma_{\mathrm{DOA}} \in [0°, 1°]$ for three representative σ values (0.1, 1, and 10), as shown in Fig. 6 and Fig. 7. For position estimation (Fig. 6), when σ is small (e.g., 0.1), the RMSE increases notably with σ_{DOA}, highlighting the sensitivity to angular accuracy. However, as σ increases, the

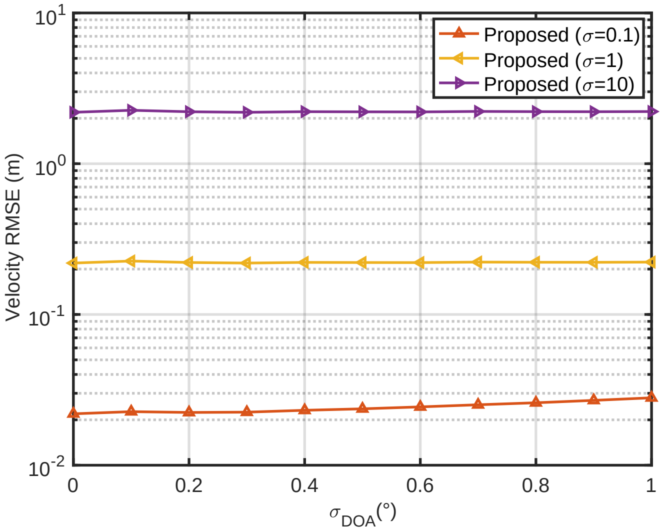

Fig. 7: Velocity RMSE comparison (angle).

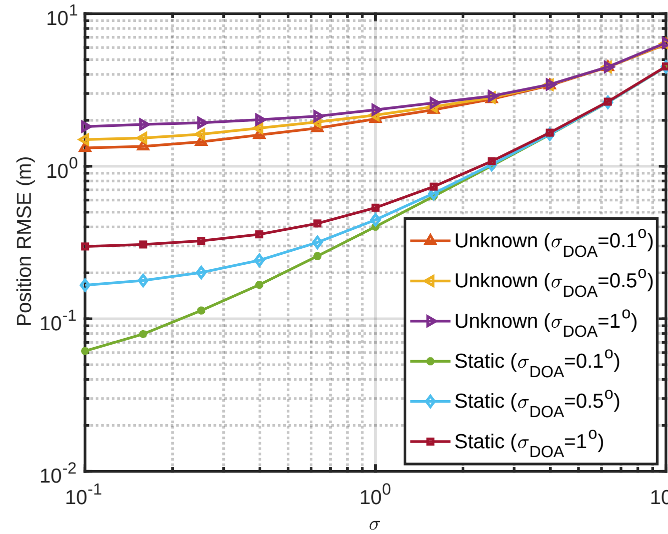

Fig. 8: Target position RMSE comparison.

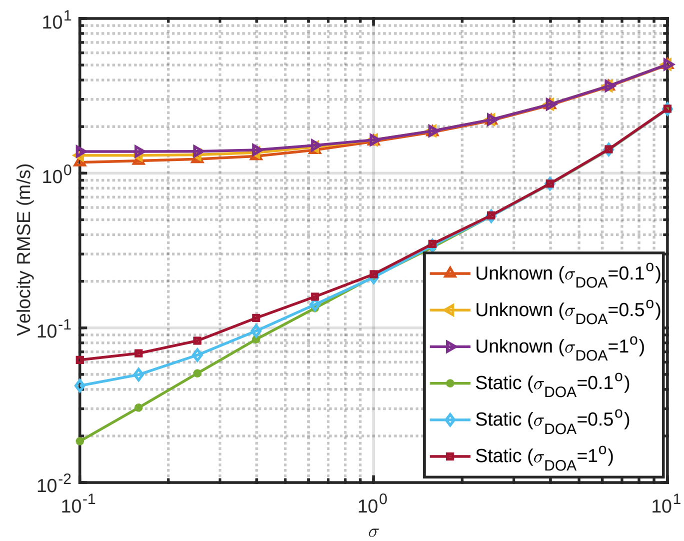

Fig. 9: Target velocity RMSE comparison.

RMSE curves flatten, showing diminishing influence of DOA error. For velocity estimation (Fig. 7), the RMSE remains nearly constant regardless of σ_{DOA}, again confirming the limited impact of angular error on velocity estimation. These results provide insight into the convergence behavior observed in Fig. 3–5, where performance differences among different σ_{DOA} settings diminish as noise levels rise.

The above results confirm the effectiveness and robustness of the proposed method under varying noise conditions. It demonstrates consistent performance improvements over the 2WLS, particularly under moderate to high noise scenarios. Moreover, the analysis reveals that while DOA errors can affect position accuracy, their influence on velocity estimation is negligible. These insights validate the practical applicability of the proposed method in dynamic TX scenarios.

B. Performance with Unknown-Location TXs

We next evaluate the performance of the proposed method when the TX positions are assumed to be unknown. Noisy $\Delta_{n,m}$, $\dot{\Delta}_{n,m}$, $\beta^{\mathrm{A}}_{n,m}$, $\psi^{\mathrm{A}}_{n,m}$, β^{TX}_{n}, and ψ^{TX}_{n} measurements are used in this case. As there are no similar approaches in the literature, we compare our proposed method with unknown-location TXs (referred to as the 'unknown location method' (Unknown)) with our previous method with static TXs in [40], referred to as the 'static location method' (Static), to evaluate the feasibility of applying the proposed method in practice. The noise settings are the same as in the dynamic-TX case, while using 4 TX–RX pairs (i.e., $N = 4$). The results are presented in Fig. 8 and Fig. 9.

The results show that the Unknown method consistently underperforms the Static method in both position and velocity estimation due to the additional uncertainty introduced by estimating TX locations. This performance gap is more pronounced under low noise conditions (small σ), where the Unknown method exhibits significantly higher RMSE values. As σ increases, the RMSEs of both methods increase, and the performance gap gradually narrows. This is because, at high noise levels, the overall error is dominated by measurement noise, and the impact of unknown TX locations becomes relatively less significant.

The analysis also reveals that the proposed method is robust against DOA noise variations. For instance, under severe DOA uncertainty ($\sigma_{\mathrm{DOA}} = 1°$), the unknown method still achieves comparable performance trends, though with consistently higher RMSEs compared to the known case. These results demonstrate that while knowledge of TX positions improves accuracy, the proposed method can still provide reasonable estimation performance when TXs are unlocalized, which is valuable for scenarios with limited infrastructure knowledge.

We also examine the performance of the unknown method in estimating the positions of unknown-location TXs. Fig. 10 presents the average position RMSE of the TXs. The results are averaged across all TXs in the system. Similar to the target localization analysis, the estimation performance deteriorates as the noise level σ increases. For low noise levels (small σ), smaller DOA noise ($\sigma_{\mathrm{DOA}} = 0.1°$) leads to noticeably

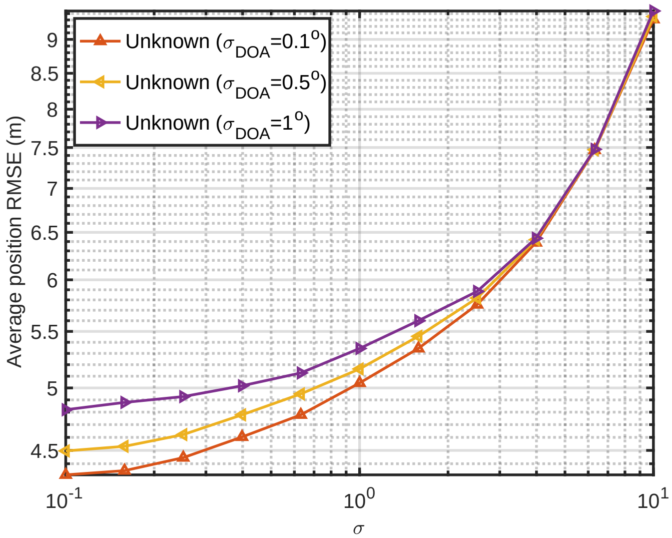

Fig. 10: TXs position RMSE comparison.

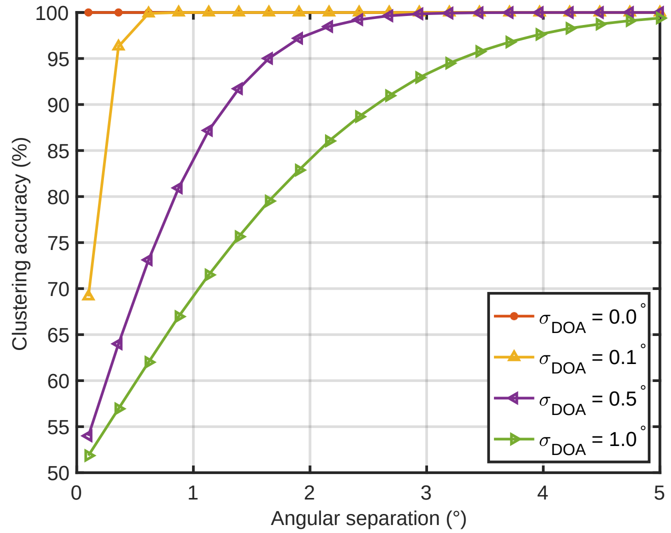

Fig. 11: Clustering accuracy versus angular separation under different DOA noise levels.

better TX localization accuracy. As σ increases, however, the RMSEs for all DOA noise levels converge, indicating that the dominant error source shifts from DOA inaccuracy to overall measurement noise.

The results suggest that even without prior knowledge of TX positions, the proposed method can achieve reasonably accurate TX localization, particularly under moderate noise conditions. This capability is important for real-world ISAC systems deployed in dynamic or infrastructure-sparse environments, where static and pre-calibrated TX positions may not be available.

The simulation results under the unknown-location TXs scenario validate the robustness and practicality of the proposed method in simultaneously estimating both the target and the TX positions. Despite the performance gap between the unknown and known TX settings, the method remains stable and effective across a wide range of noise levels. In particular, the position and velocity estimation performance converge to that of the known-TX benchmark as the noise level increases, suggesting that the relative impact of missing TX information diminishes under high-noise conditions. Furthermore, the method demonstrates reliable TX localization accuracy, which is essential for enabling self-organizing ISAC systems without requiring prior TX calibration.

C. Impact of Angular Separation on Target Distinguishability

As discussed in Section II.D, for multiple-target localization, we decompose the problem into multiple independent single-target localizations. This approach relies on the assumption that all targets are spatially separable in the angular domain so that the RX can distinguish the corresponding measurement groups for each target. However, this distinguishability depends jointly on the angular separation between targets and the DOA measurement noise.

To examine this effect, we simulate two targets with angular separations in the range $[0.1^\circ, 5^\circ]$ under four representative noise levels $\sigma_{\text{DOA}} \in 0^\circ, 0.1^\circ, 0.5^\circ, 1^\circ$. With three TX–RX pairs, the RX receives two measurement groups from each pair, corresponding to the two targets. Each group contains the BR, BRR, and DOA measurements associated with one target. Since the RX does not know a priori which group corresponds to which target, the six mixed groups must be partitioned into two target-specific sets. We apply the standard K-means clustering algorithm [45] to assign each measurement group to its corresponding target based on its DOA features. The resulting clustering accuracy is shown in Fig. 11. As illustrated in Fig. 11, when the DOA measurements are noise-free, the clustering accuracy remains 100% even for extremely small angular separations, indicating that grouping ambiguity is primarily induced by noise. With mild noise ($\sigma_{\text{DOA}} = 0.1^\circ$), near-perfect distinguishability is achieved once the separation exceeds approximately 0.5°. For moderate and strong noise levels ($\sigma_{\text{DOA}} = 0.5^\circ$ and 1°), the clustering accuracy increases monotonically with angular separation. In particular, accuracy above 95% is obtained when the separation exceeds roughly 2° for $\sigma_{\text{DOA}} = 0.5^\circ$, while $\sigma_{\text{DOA}} = 1^\circ$ requires separations above 4° to reach similar performance.

These results provide an empirical guideline for determining when multi-target scenarios can be reliably decomposed into independent single-target localization problems. In environments with moderate DOA noise, separations of a few degrees are sufficient to ensure high distinguishability, whereas very closely spaced targets or high-noise conditions may require more advanced grouping or joint-estimation strategies.

Finally, it is important to note that practical radar systems are also constrained by their intrinsic angular resolution. If the resolution is insufficient, multiple physically separated targets may appear as a single peak before any localization processing occurs. Such front-end ambiguities arise from hardware limitations rather than the geometric estimation model considered in this work. Since our focus is on the post-measurement geometric estimation stage, scenarios in which the sensing front-end cannot resolve multiple targets are beyond the scope of this paper.

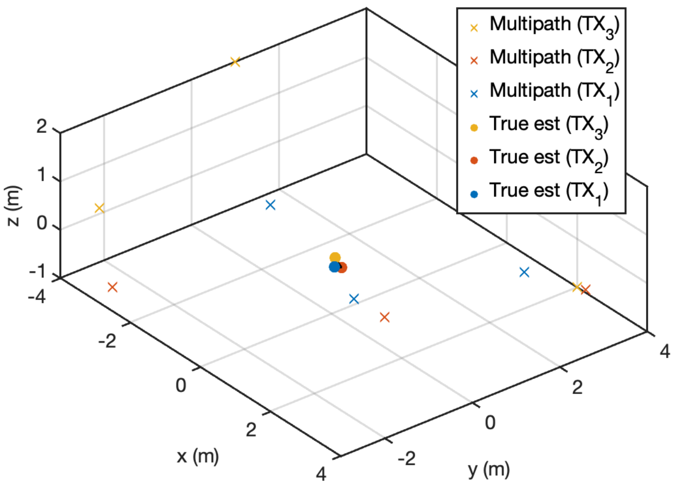

Fig. 12: True versus multipath-induced target estimates.

D. Impact of Multipath-Induced Ghost Targets

The system model in Fig. 1 considers only the direct path and the strongest reflection from targets, without explicitly modeling complex multipath propagation. In practice, additional reflections—particularly those involving walls, furniture, or other surrounding structures—may generate ghost targets that do not correspond to the true physical object. These ghost targets introduce extra BR, BRR, and DOA values that violate the geometric constraints of the actual TX–target–RX configuration, thereby increasing the difficulty of distinguishing true targets.

To examine the impact of such multipath-induced ghost targets, we extend the original study by injecting additional non-line-of-sight (NLOS) observations for each TX–RX pair. Importantly, the proposed localization framework inherently relies on geometric consistency across different TX–RX pairs. As each pair experiences its own multipath propagation environment, the resulting ghost measurements fail to form a consistent triangulation in 3D space. Consequently, estimates obtained from true target measurements naturally converge into a tight and coherent cluster across all TX–RX pairs, whereas estimates generated from multipath observations remain spatially dispersed.

This effect is demonstrated in Fig. 12, which considers three TX–RX pairs. For each pair, one true measurement and three multipath-induced ghost measurements are generated. The localization results associated with the true target (shown as colored solid markers) form a compact cluster around the actual target location. In contrast, the estimates derived from multipath measurements (shown as cross markers) scatter widely throughout the 3D space and exhibit no geometric consistency. This spatial divergence provides a simple and effective cue for identifying and rejecting multipath-induced ghost estimates. In practice, this robustness arises naturally from the geometric-consistency requirement of our algorithm: true estimates remain tightly clustered across TX–RX pairs, whereas ghost estimates do not. Thus, a practical rejection rule can be implemented by setting a threshold on the spread of localization results across different TXs, where estimates exceeding this divergence threshold are classified as multipath-induced ghosts.

V. Conclusion

In this paper, we proposed two localization algorithms for tracking a moving target in a multistatic ISAC system, addressing two challenging scenarios: dynamic transmitters and unknown-location transmitters. Both algorithms utilize BR, BRR, and DOA measurements acquired by a static RX equipped with an antenna array. In the dynamic TX scenario, the proposed method enables accurate position and velocity estimation even with a single TX-RX pair, and shows superior performance compared to a representative BR/BRR-based baseline. In the unknown-location TX scenario, our approach is the first to jointly estimate the positions of both the target and the transmitters without prior TX knowledge. Simulation results confirm the robustness and accuracy of the proposed methods under various noise levels and DOA conditions.

As directions for future work, we plan to extend the proposed algorithms to more complex multi-target environments with ambiguous or overlapping DOAs, where data association and measurement disambiguation become critical. Additionally, we aim to implement and validate our methods on a real-world hardware platform to assess their practical feasibility and robustness under non-ideal conditions.

References

[1] F. Liu, Y. Cui, J. Xu, T. X. Han, Y. C. Eldar, and S. Buzzi, “Integrated sensing and communications: Towards dual-functional wireless networks for 6g and beyond,” *IEEE Journal on Selected Areas in Communications*, 2022.
[2] 3GPP, “Feasibility study on integrated sensing and communication,” Tech. Rep., 2024.
[3] F. Liu, C. Masouros, A. P. Petropulu, H. Griffiths, and L. Hanzo, “Joint radar and communication design: Applications, state-of-the-art, and the road ahead,” *IEEE Transactions on Communications*, 2020.
[4] Z. Cui, J. Hu, J. Cheng, and G. Li, “Multi-domain noma for isac: Utilizing the dof in the delay-doppler domain,” *IEEE Communications Letters*, 2023.
[5] K. Kim, J. Kim, and J. Joung, “A survey on system configurations of integrated sensing and communication systems,” in *Proc. ICTC*, 2022.
[6] T. Wild, V. Braun, and H. Viswanathan, “Joint design of communication and sensing for beyond 5g and 6g systems,” *IEEE Access*, 2021.
[7] H. Wymeersch *et al.*, “Deliverable d3.3: Final models and measurements for localisation and sensing,” Tech. Rep., 2023.
[8] Y. Zeng, Y. Ma, and S. Sun, “Joint radar-communication with cyclic prefixed single carrier waveforms,” *IEEE Transactions on Vehicular Technology*, 2020.
[9] S. Cai, L. Chen, Y. Chen, H. Yin, and W. Wang, “Pulse-based isac: Data recovery and ranging estimation for multi-path fading channels,” *IEEE Transactions on Communications*, 2023.
[10] Y. Zeng, Y. Ma, and S. Sun, “Joint radar-communication: Low complexity algorithm and self-interference cancellation,” in *Proc. IEEE Globecom*, 2018.
[11] B. Li, W. Ni, and H. Wymeersch, “Integrated sensing and communication: A perspective on security,” *IEEE Wireless Communications*, 2021.
[12] A. Liu, V. Misra, and D. Agrawal, “Joint waveform design and beamforming for integrated sensing and communication systems,” *IEEE Transactions on Wireless Communications*, 2021.
[13] S. Wu, L. Li, Y. Chen, and M. Renzo, “Joint radar and communication waveform design for isac systems with reconfigurable intelligent surfaces,” *IEEE Transactions on Signal Processing*, 2021.
[14] J. Zhang, Z. Liu, Y. Zhang, and K. Huang, “Unified waveform design for integrated sensing and communication in 6g networks,” *IEEE Transactions on Wireless Communications*, 2021.
[15] K. Zhang, H. Guo, S. Leng, and Q. Yang, “Joint communication and sensing beamforming in mmwave isac systems,” in *Proc. IEEE Globecom*, 2022.

[16] M. Polese, F. Chiarotti, and M. Zorzi, “Localization in integrated sensing and communication systems: A survey and future directions,” *IEEE Communications Surveys & Tutorials*, 2021.
[17] C. B. Barneto, M. Turunen, S. D. Liyanaarachchi, L. Anttila, A. Brihuega, T. Riihonen, and M. Valkama, “High-accuracy radio sensing in 5g new radio networks: Prospects and self-interference challenge,” in *Proc. Asilomar Conference on Signals, Systems and Computers*, 2019.
[18] A. Bharadwaj *et al.*, “Positioning and sensing in 6g: Gaps, challenges, and opportunities,” *IEEE Vehicular Technology Magazine*, 2023.
[19] D. A. Gray, “Bistatic radar: Principle and practice,” *IEEE Transactions on Aerospace and Electronic Systems*, 2019.
[20] X. Zhang, Y. Ma, Y. Zeng, S. Sun, and Y. Wang, “Bistatic joint radar and communication with 5g signal for range speed angle detections,” in *Proc. IEEE VTC-Fall*, 2023.
[21] F. Colone, D. H. He, and P. Lombardo, “Multistatic passive radar systems: Achievements and challenges,” *IEEE Aerospace and Electronic Systems Magazine*, 2021.
[22] P. Angeletti, G. Galati, and M. Martorella, “Bistatic and multistatic radar imaging: Theory and practice,” *IEEE Transactions on Geoscience and Remote Sensing*, 2020.
[23] H. Griffiths and C. Baker, “An introduction to bistatic and multistatic radar systems,” *IEEE Aerospace and Electronic Systems Magazine*, 2020.
[24] F. Zhang, Y. Sun, J. Zou, D. Zhang, and Q. Wan, “Closed-form localization method for moving target in passive multistatic radar network,” *IEEE Sensors Journal*, 2020.
[25] R. Amiri, F. Behnia, and M. A. M. Sadr, “Efficient positioning in mimo radars with widely separated antennas,” *IEEE Communications Letters*, 2017.
[26] ——, “Exact solution for elliptic localization in distributed mimo radar systems,” *IEEE Transactions on Vehicular Technology*, 2018.
[27] F. Zhang, Y. Sun, and Q. Wan, “Calibrating the error from sensor position uncertainty in tdoa-aoa localization,” *Signal Processing*, 2020.
[28] Y. S. Zhao, Y. J. Zhao, and C. Zhao, “A novel algebraic solution for moving target localization in multi-transmitter multi-receiver passive radar,” *Signal Processing*, 2018.
[29] Y. Sun, K. C. Ho, and Q. Wan, “Solution and analysis of tdoa localization of a near or distant source in closed form,” *IEEE Transactions on Signal Processing*, 2019.
[30] Y. Sun, F. Zhang, and Q. Wan, “Wireless sensor network-based localization using tdoa measurements in mpr,” *IEEE Sensors Journal*, 2019.
[31] S. Chang, Y. Li, X. Xing, H. Wang, W. Wu, and Y. Yu, “A novel localization method based on rss-aoa combined measurements by using polarized identity,” *IEEE Sensors Journal*, 2017.
[32] H. Yang and J. Chun, “An improved algebraic solution for moving target localization in noncoherent mimo radar systems,” *IEEE Transactions on Signal Processing*, 2016.
[33] H. Xiong, M. Peng, S. Gong, and Z. Du, “A novel hybrid rss and toa positioning algorithm for multi-objective cooperative wireless sensor networks,” *IEEE Sensors Journal*, 2018.
[34] K. C. Ho and W. Xu, “An accurate algebraic solution for moving source location using tdoa and fdoa measurements,” *IEEE Transactions on Signal Processing*, 2004.
[35] C. H. Park and J. H. Chang, “Closed-form localization for distributed mimo radar systems using time delay measurements,” *IEEE Transactions on Wireless Communications*, 2016.
[36] Z. Mao, H. Su, B. He, and X. Jing, “Moving source localization in passive sensor network with location uncertainty,” *IEEE Signal Processing Letters*, 2021.
[37] S. A. R. Kazemi, R. Amimi, and F. Behnia, “Efficient joint localization and synchronization in distributed mimo radars,” *IEEE Signal Processing Letters*, 2020.
[38] T. Sun and Z. H. Yu, “Moving target localization in distributed mimo radar systems with sensor position errors in the presence of a calibration object,” *Digital Signal Processing*, 2022.
[39] T. Sun and W. Wang, “Efficient multistatic radar localization algorithms for a uniformly accelerated moving object with sensor parameter errors,” *IEEE Transactions on Aerospace and Electronic Systems*, 2023.
[40] S. Zhuge, Y. Ma, Z. Lin, and Y. Zeng, “A novel geometric solution for moving target localization through multistatic sensing in the isac system,” in *Proc. IEEE VTC-Spring*, 2024.
[41] Q. Yuan, S. Zhuge, Z. Lin, Y. Ma, and Y. Zeng, “Kalman filtering based target tracking for multistatic sensing in isac systems,” in *IEEE International Symposium on Circuits and Systems (ISCAS)*, 2025.
[42] J. A. Zhang, F. Liu, C. Masouros, R. W. Heath, Z. Feng, L. Zheng, and A. Petropulu, “An overview of signal processing techniques for joint communication and radar sensing,” *IEEE Journal of Selected Topics in Signal Processing*, 2021.
[43] N. K. Nataraja, S. Sharma, K. Ali, F. Bai, R. Wang, and A. F. Molisch, “Integrated sensing and communication (isac) for vehicles: Bistatic radar with 5g-nr signals,” *IEEE Transactions on Vehicular Technology*, 2025.
[44] A. Kaushik, E. Vlachos, J. Thompson, M. Nekovee, and F. Coutts, “Towards 6g: Spectrally efficient joint radar and communication with radio frequency selection, interference and hardware impairments (invited paper),” *IET Signal Processing*, 2022.
[45] S. Lloyd, “Least squares quantization in pcm,” *IEEE Transactions on Information Theory*, 1982.

Shun Zhuge (Student Member, IEEE) received the B.Eng. (Hons.) degree in Electronic and Communication Systems from the Australian National University, Australia, in 2022, and the M.Sc. degree in Communications Engineering from Nanyang Technological University, Singapore, in 2024. During his master’s study, he conducted research in collaboration with the Institute for Infocomm Research (I²R), A*STAR, Singapore. He is currently pursuing the Ph.D. degree at Delft University of Technology, the Netherlands. His research interests include integrated sensing and communication, wireless localization, and antenna array signal processing.

Yugang Ma (Senior Member, IEEE) received the B.S. degree in Radio Engineering and the M.S. degree in Computer Engineering from Chongqing University, China, and the Ph.D. degree in Telecommunications Engineering from the University of Electronic Science and Technology of China (UESTC). Since 2013, Dr. Ma has been with the Institute for Infocomm Research (I²R), A*STAR, Singapore, where he is currently a Senior Principal Scientist. He previously held the role of Group Leader for white space communications research. Prior to joining I²R, he spent 13 years at Sony Electronics, where he was recognized as a Distinguished Engineer and received eight patent awards. His research expertise encompasses communications and radar systems, deep learning, MIMO technology, integrated sensing and communications, localization, dynamic spectrum access, time synchronization, interference suppression, and antenna technologies. Dr. Ma holds over 50 granted patents and was a recipient of the Singapore Manufacturing Federation Award (2014). Additionally, he has held several editorial roles within the IMDA TSAC WG6, including the Chief Editors of taskforces for IoT LoRa (2016–2017), NB-IoT (2018–2019), and the Editor for 5G NR CBS CMT (2020–2021).

Zhiping Lin (Life Senior Member, IEEE) received the Ph.D. degree in Information Engineering from the University of Cambridge, UK, in 1987. Since 1999, he has been an associate professor at the School of EEE, Nanyang Technological University (NTU), Singapore, where he is now serving as the Programme Director of the Master of Science in Signal Processing and Machine Learning, the School of EEE, NTU. Prior to that, he worked at DSO National Labs, Singapore and Shantou University, China. Dr. Lin was the Editor-in-Chief of Multidimensional Systems and Signal Processing from 2011 to 2015, a subject editor of the Journal of the Franklin Institute of from 2025 to 2020, and he also served as an associate editor for several other international journals. He was IEEE CASS Distinguished Lecturer, and served/is serving as IEEE CASS and SPS Singapore Chapter Chairs. His research interests include signal processing and machine learning. He has published more than 250 peer-reviewed journal papers.

Yonghong Zeng (Fellow, IEEE) received the B.S. degree from Peking University and the M.S. and Ph.D. degrees from the National University of Defense Technology, China. He was with the National University of Defense Technology, Nanyang Technological University, and The University of Hong Kong, as an Assistant/Associate Professor or a Research Fellow. He has been with the Institute for Infocomm Research (I²R), A*STAR, since 2004, and is currently a Senior Principal Scientist and technical advisor. He is working on integrated sensing and communication, B5G/6G communications, ultra-reliable low-latency communication, vehicular radar and communication, and real time localization systems. He received the 2007 and 2009 IES (Institute of Engineers Singapore) Prestigious Engineering Achievement Award in Singapore and the Ministry-Level Scientific and Technological Development Award four times in China. He received the Award for Advances in Communication from the IEEE Communication Society in 2022, the Inaugural IEEE Communications Society Asia–Pacific Best Paper Award in 2012, and a few other best paper awards. He received the Certificate of Appreciation for outstanding contributions to the IEEE 802.22 Standard in 2011.